# Hole tunneling through the emitter-base junction of a heterojunction bipolar transistor

T. Kumar, M. Cahay, and K. Roenker
*Department of Electrical Engineering, University of Cincinnati, Cincinnati, Ohio 45221*
(Received 18 February 1997; revised manuscript received 17 April 1997)

Starting with the $4\times4$ Luttinger-Kohn Hamiltonian, we develop a scattering-matrix approach to study coherent hole transport through the valence-band energy profile across the emitter-base junction of typical abrupt and graded *Pnp* heterojunction bipolar transistors. The tunneling and reflection coefficients of heavy and light holes are calculated for the upper and lower $2\times2$ Hamiltonians obtained through a unitary transform of the $4\times4$ Luttinger-Kohn Hamiltonian. The probability for a transition from heavy (light) to light (heavy) hole while tunneling across the emitter-base junction is calculated as a function of the value of the wave vector parallel to the emitter-base heterointerface for both abrupt and graded heterojunctions. For holes injected from the emitter into the base, the probability of heavy- to light-hole conversion is shown to be quite different when calculated with the upper and lower Hamiltonians. On the other hand, the probability of light- to heavy-hole conversion is nearly the same for the upper and lower Hamiltonians. The energy dependence of the heavy- and light-hole tunneling coefficients is shown to be quite different from those calculated using a parabolic-band model, in which the effects of mixing and anisotropy in the valence band are neglected. [S0163-1829(97)07431-6]

## I. INTRODUCTION

The utility of *Pnp* bipolar transistors are well known from silicon-integrated circuits. *Pnp* transistors find applications as active loads where they provide higher gain with reduced parasitics and as complementary transistors in push-pull amplifiers for power applications. The development of *Pnp* GaAs- and InP-based heterojunction bipolar transistors (HBT's) has received increased interest only over the last few years.[1] For example, Enquist, Slater, and Stuart[2] demonstrated $Al_xGa_{1-x}As$/GaAs *Pnp* transistors with gains up to 300 at a collector current density of $1.5\times10^4$ A/cm$^2$ with an $f_T$ of 21 GHz and an $f_{max}$ of 23 GHz. Based on these devices, they demonstrated a low-power, high-speed, complementary HBT-based, integrated injection logic with 65 ps and 13 mW per gate for a speed-power product of 850 fJ. More recently, they[3] fabricated $Al_xGa_{1-x}As$/GaAs *Pnp* HBT's with thin base and collector regions and reported values of $f_T$ and $f_{max}$ of 33 and 66 GHz, respectively. Hill *et al.*[4] and Liu *et al.*[5] obtained *Pnp*'s with a current gain of 200, an $f_T$ of 23 GHz, and an $f_{max}$ of 40 GHz, and demonstrated a push-pull power amplifier at 10 GHz with an output power of 500 mW with a 6-dB gain and a 41.8% power-added efficiency. For InP-based HBT's, there have been only a few reports of *Pnp* HBT's while high-performance *Npn* transistors have been widely reported.[6,7] Stanchina *et al.*[8] obtained a current gain of 25, an $f_T$ of 10 GHz, and an $f_{max}$ of 27 GHz at $7\times10^3$ A/cm$^2$ for an $In_xAl_xAs/In_xGa_{1-x}As$ *Pnp* transistor. Similarly, Lunardi, Chandrasekhar, and Hamm[9] reported a current gain of 420 with an $f_T$ of 10.5 GHz and an $f_{max}$ of 25 GHz for an InP/$In_xGa_{1-x}As$ *Pnp* HBT.

In view of their potential for a wide variety of applications, there is a need to develop accurate models of the device physics of *Pnp* HBT's. While the importance of electron tunneling through the emitter-base spike of Npn HBT's has been investigated by several groups,[10–13] the importance of hole tunneling across the emitter-base junction of abrupt and graded *Pnp* HBT's has not been addressed so far, to our knowledge. This paper presents a treatment of coherent transport of hole through the emitter-base junction of *Pnp* HBT's with abrupt and graded interfaces, while taking into account the effects of valence-band anisotropy and mixing between heavy and light holes.

In the past, there have been only a few reports of the treatment of hole tunneling in realistic structures based on the transfer-matrix formalism following the original $\mathbf{k}\cdot\mathbf{p}$ model.[14] Starting with the Luttinger-Kohn Hamiltonian, Chuang used a transfer-matrix approach to study the problem of hole tunneling through simple potential steps.[15] He showed that there is a high probability for a hole to change character (heavy to light or the reverse) while tunneling from the low gap to higher band-gap material at a heterojunction interface. On the other hand, the probability of conversion from heavy to light or the reverse is much less for holes incident on an interface from the higher band-gap material. Other studies have investigated applications of the transfer-matrix formalism to the problem of hole tunneling in resonant tunneling structures.[16–19] These simulations showed that the transfer-matrix method is numerically unstable for device structures larger than a few tens of Å. To circumvent the difficulties encountered in the transfer-matrix technique, Liu, Ting, and McGill recently proposed the use of the multiband quantum transmitting boundary method (MQTBM).[20] This technique is easy to implement, numerically stable, and as numerically efficient as the transfer-matrix technique. So far, Liu, Ting, and McGill have applied their MQTBM technique only to hole transport through resonant tunneling devices.

In this paper, we develop a scattering-matrix technique to study coherent hole transport through the emitter-base junction of abrupt and graded *Pnp* HBT's. The scattering-matrix technique has been applied extensively in the past to study electron transport through submicron and mesoscopic

 

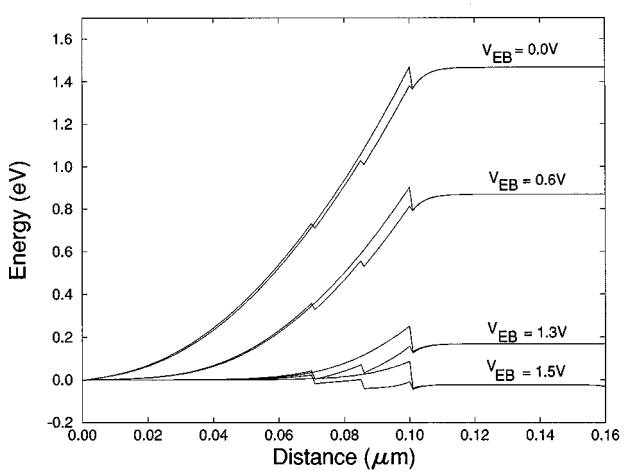


FIG. 1. Valence-band energy profile across the emitter-base junction of typical abrupt and graded *Pnp* HBT under forward-bias operation. Hole energies are measured positive, as indicated on the figure, while taking the valence-band energy profile in the bulk of the emitter region as the zero of energy. In the graded HBT, the emitter consists of a 700-Å-long *P*-type $Al_{0.3}Ga_{0.7}As$ region doped at $2\times10^{17}$ $cm^{-3}$ on top of a 300-Å $Al_xGa_{1-x}As$ graded region with the same doping level. The graded region consists of two regions of $Al_xGa_{1-x}As$ with $x=0.2$ and 0.1 going from emitter to base, each region being 150 Å wide. The base region consists of a 600-Å heavily doped ($5\times10^{18}$ $cm^{-3}$) *N*-type region. Also shown is the valence-band profile in an abrupt HBT in which the emitter consists of 1000 Å of *P*-type $Al_{0.3}Ga_{0.7}As$ doped at $2\times10^{17}$ $cm^{-3}$, the rest of the structure being unchanged.

systems[21,22] and is known to remain stable and accurate for large systems. A scattering-matrix approach was used earlier by Ko and Ickson[23] to study multiband electron transport in extended nonperiodic structures. They applied their technique to study resonant tunneling in $GaAs/Al_xGa_{1-x}As$ multilayer systems with the higher band-structure minima included. Their results show that the resonance transmissions are readily separated into the GaAs Γ-well resonances and the AlAs *X*-well resonances. The scattering matrix to describe hole transport has also been used recently by Sanchez and Proetto,[24] but they only considered the tunneling of holes across simple barriers and above quantum wells about 5 nm wide.

Hereafter, we consider hole tunneling through the emitter-base valence-band energy profile of typical *Pnp* HBT's, such as the one shown in Fig. 1. In this figure, the valence-band energy profile is drawn such that the incident (kinetic) energy of the hole is positive, as indicated in the figure with the top of the valence-band energy profile in the emitter selected as the zero of energy. For the III-V compound materials considered here, the presence of the split-off band, typically over 300 meV below the maximum of the valence-band region, could lead to a finite probability for heavy (or light) hole to split-off band transitions for holes tunneling from the emitter to base, especially at a large forward emitter-base bias. At a low forward emitter-base bias, the tunneling of holes from emitter to base should also include the presence of the split-off band in the emitter, since the maximum of the latter is located below the maximum of the valence band in the base at low bias. Therefore, to avoid complications linked to the presence of the split-off bands on either side of the junction, we limit our investigations of hole tunneling to the fairly large forward-bias case and to an energy range below the maximum of the split-off band in the base region. This corresponds to a forward-bias emitter base between 1.3 and 1.5 V for the $Al_{0.3}Ga_{0.7}As/GaAs$ structure shown in Fig. 1, and between 0.7 and 0.9 V for the $In_{0.52}Al_{0.48}As/In_{0.53}Ga_{0.47}As$ structure considered in our numerical examples. These are the practical ranges of bias at which these *Pnp* HBT's must be operated to show large dc current gain and unity gain cut-off frequency.

This paper is organized as follows. In Sec. II, the transmission and reflection coefficients of heavy and light holes are calculated for the upper and lower $2\times2$ Hamiltonians obtained through a unitary transform of the $4\times4$ Luttinger-Kohn Hamiltonian. Starting with the $2\times2$ Hamiltonians, we develop the scattering-matrix formalism to describe hole tunneling through an arbitrary valence-band energy profile. In Sec. III, we discuss numerical examples illustrating the effects of band mixing between heavy and light holes on the tunneling of holes through the emitter-base junction of typical *Pnp* HBT's. Finally, Sec. IV contains our conclusions.

## II. APPROACH

Following Chuang,[15] we start with the well-known Luttinger-Kohn Hamiltonian[25] describing the top of the valence band while ignoring the split-off band,

$$H=\begin{bmatrix} P+Q & -S & R & 0 \\ -S^{\dagger} & P-Q & 0 & R \\ R^{\dagger} & 0 & P-Q & S \\ 0 & R^{\dagger} & S^{\dagger} & P+Q \end{bmatrix}, \tag{1}$$

where † stands for the complex conjugate. In writing the Hamiltonian above, the energy of holes is measured positive as indicated in Fig. 1. The explicit expressions for the above matrix elements are

$$P=\Gamma_1(k_x^2+k_y^2+k_z^2), \quad Q=\Gamma_2(k_x^2+k_y^2-2k_z^2), \tag{2}$$

$$R=-\sqrt{3}\tilde{\Gamma}(k_x-ik_y)^2+\sqrt{3}\left[\frac{\Gamma_3-\Gamma_2}{2}\right](k_x+ik_y)^2,$$

$$S=2\sqrt{3}\Gamma_3(k_x-ik_y)k_z, \tag{3}$$

where $\Gamma_1=\hbar^2\gamma_1/2m_0$, $\Gamma_2=\hbar^2\gamma_2/2m_0$, $\Gamma_3=\hbar^2\gamma_3/2m_0$, and $\tilde{\Gamma}=(\Gamma_2+\Gamma_3)/2$, the $\gamma_i$'s are the Luttinger parameters,[25] and $m_0$ is the free-electron mass.

The Hamiltonian in Eq. (1) is a $4\times4$ matrix in the basis $(|\frac{3}{2},\frac{3}{2}\rangle, |\frac{3}{2},\frac{1}{2}\rangle, |\frac{3}{2},-\frac{1}{2}\rangle, |\frac{3}{2},-\frac{3}{2}\rangle)$ of the four degenerate Bloch wave functions at the center of the Brillouin zone. These basis functions are given explicitly in the appendix of Ref. 15. The $4\times4$ Luttinger-Kohn Hamiltonian (1) can be block diagonalized using a unitary transformation[15]

$$H=\begin{bmatrix} H^U & 0 \\ 0 & H^L \end{bmatrix},$$

where the upper and the lower blocks are given by

$$H^{\sigma}=\begin{bmatrix} P\pm Q & \widetilde{R} \\ \widetilde{R}^{\dagger} & P\mp Q \end{bmatrix}, \tag{4}$$

where $\sigma=U$ (or $L$) refers to the upper (or lower) $\pm$ signs. In the expressions of $H^L$ and $H^U$, $\widetilde{R}$ is equal to $|R|-i|S|$, where $R$ and $S$ have been defined above.

In the numerical examples below, the diagonal elements in Eq. (4) will usually contain an extra potential-energy term which can easily be incorporated in the expressions given below for the energy eigenvalues and corresponding wave vectors for heavy and light holes. Hereafter, we focus only on the $H^U$ part of the Hamiltonian, whose eigenvalues are given by

$$E(k)=Ak^2\pm[B^2k^4+C^2(k_x^2k_y^2+k_y^2k_z^2+k_x^2k_z^2)]^{1/2}, \tag{5}$$

where $A=\Gamma_1$, $B=2\Gamma_2$, $C^2=12(\Gamma_3^2-\Gamma_2^2)$, and $k^2=k_x^2+k_y^2+k_z^2$ and the $+$ and $-$ signs refer to light (LH) and heavy (HH) holes, respectively. For simplicity, we consider the $(k_x,k_z)$ plane, and set $k_y$ equal to zero. As a result, rearranging Eq. (5), we obtain

$$k_z^2(k_x,E)=\frac{1}{A^2-B^2}\left\{AE-\left(A^2-B^2-\frac{C^2}{2}\right)k_x^2 \mp\left[B^2E^2+AC^2Ek_x^2 - C^2\left(A^2-B^2-\frac{C^2}{4}\right)k_x^4\right]^{1/2}\right\}, \tag{6}$$

where the $+$ is for the heavy hole and the $-$ is for the light hole. We chose the $z$ axis as the direction of growth of the heterostructure, and we focus on hole injection from emitter to base.

The corresponding eigenvectors for the HH and LH wave functions are[15]

$$\psi_{\mathrm{HH}}(r)=\frac{1}{N}\begin{bmatrix} U \\ -\widetilde{R}^{\dagger}\end{bmatrix}=\begin{bmatrix} F_{1H} \\ F_{2H}\end{bmatrix}e^{i\mathbf{k}\cdot\mathbf{r}} \tag{7}$$

and

$$\psi_{\mathrm{LH}}(r)=\frac{1}{N}\begin{bmatrix} \widetilde{R} \\ U\end{bmatrix}=\begin{bmatrix} F_{1L} \\ F_{2L}\end{bmatrix}e^{i\mathbf{k}\cdot\mathbf{r}}, \tag{8}$$

where

$$U=(Q^2+\widetilde{R}\widetilde{R}^{\dagger})^{1/2}-Q=\begin{Bmatrix} P-Q-E(\mathrm{HH}) \\ E-P-Q(\mathrm{LH})\end{Bmatrix}, \tag{9}$$

and

$$N=(|U|^2+|\widetilde{R}|^2)^{1/2} \tag{10}$$

is a normalization constant.

An arbitrary valence-band energy profile can always be approximated as a series of small steps in which the valence-band edge is assumed to be a constant. While considering tunneling between the contacts sandwiching an arbitrary heterostructure, the wave function of a heavy hole incident from the left contact can be written[15]

$$\psi_{\mathrm{HH}}(\mathbf{r})=\begin{bmatrix} F_{1H} \\ F_{2H}\end{bmatrix}e^{i(k_xx+k_z^{(h)}z)}, \tag{11}$$

where $F_{1H}=U_H/N_H=(P_H-Q_H-E)/N_H$, $F_{2H}=R_H^{\dagger}/N_H$, and $N_H=\sqrt{|P_H-Q_H-E|^2+|\widetilde{R}_H|^2}$. The quantities $P_H$, $Q_H$, $U_H$, and $\widetilde{R}_H$ are the expressions given above evaluated for $k_z=k_z^{(H)}$ in Eq. (6). The reflected wave can be written as

$$\psi_{\mathrm{refl}}(\mathbf{r})=\Gamma_{\mathrm{HH}}\begin{bmatrix} F_{1H} \\ F_{2H}^{-}\end{bmatrix}e^{i(k_xx-k_z^{(h)}z)}+\Gamma_{\mathrm{LH}}\begin{bmatrix} F_{1L}^{-} \\ F_{2L}\end{bmatrix}e^{i(k_xx-k_z^{(l)}z)}, \tag{12}$$

where $\Gamma_{\mathrm{HH}}$ and $\Gamma_{\mathrm{LH}}$ are the reflection amplitudes for the heavy and light holes, respectively, $F_{1L}^{-}=\widetilde{R}_L(-k_z^{(L)})/N_L$, $F_{2H}^{-}=-\widetilde{R}_H^{\dagger}(-k_z^{(H)})/N_H$, and $F_{2L}=U_L/N_L$. The quantities $P_L$, $Q_L$, $R_L$, $U_L$, and $N_L$ are the values of the $(P,Q,R,U,N)$ expressions evaluated for $k_z=k_z^{(L)}$. On the other hand, the transmitted wave function can be written

$$\psi_{\mathrm{trans}}(\mathbf{r})=\tau_{\mathrm{HH}}\begin{bmatrix} F_{1H}^{t} \\ F_{2H}^{t}\end{bmatrix}e^{i(k_xx+k_{tz}^{(h)}z)}+\tau_{\mathrm{LH}}\begin{bmatrix} F_{1L}^{t} \\ F_{2L}^{t}\end{bmatrix}e^{i(k_xx+k_{tz}^{(l)}z)}, \tag{13}$$

where the superscript $t$ is a reminder that the quantities must be evaluated in the transmitted region (the base of the transistor in our case). In Eq. (13), $\tau_{\mathrm{LH}}$ and $\tau_{\mathrm{HH}}$ are the transmission coefficients for the light and heavy holes, respectively.

At the interface between any two steps approximating the valence-band energy profile, the envelope functions $F_{1,2}(z)$ must be chosen such that

$$\begin{bmatrix} F_1(z) \\ F(z)\end{bmatrix}\quad\text{and}\quad\begin{bmatrix} (\Gamma_1-2\Gamma_2)\dfrac{\partial}{\partial z} & \sqrt{3}\Gamma_3k_x \\ -\sqrt{3}\Gamma_3k_x & (\Gamma_1+2\Gamma_2)\dfrac{\partial}{\partial z}\end{bmatrix}\begin{bmatrix} F_1(z) \\ F_2(z)\end{bmatrix} \tag{14}$$

are continuous.[26] Applying these boundary conditions across each potential step in the valence band, the unknown reflection and transmission amplitudes $\Gamma_{\mathrm{HH}}$, $\Gamma_{\mathrm{LH}}$, $\tau_{\mathrm{HH}}$, and $\tau_{\mathrm{LH}}$ can then be found as solutions of the matrix equation

$$M[\Gamma_{\mathrm{HH}},\Gamma_{\mathrm{LH}},\tau_{\mathrm{HH}},\tau_{\mathrm{LH}}]^T=\mathbf{V}_h, \tag{15}$$

where $T$ stands for the transpose operation, and the explicit forms of $M$ and $\mathbf{V}_h$ are given in Ref. 17. Repeating the analysis above while shooting the heavy hole from right to left, the corresponding reflection and transmission amplitudes can be found to obey an equation similar to Eq. (15). We denote these reverse reflection and transmission coefficients with a prime. After repeating the above analysis for a light hole incident from either side, we then can form the scattering matrix $S$ across a potential step which relates the incoming and outgoing amplitudes of the hole wave functions on either side of each potential step as follows:

$$S=\begin{bmatrix} \tau & \rho' \\ \rho & \tau'\end{bmatrix}, \tag{16}$$

where

$$\tau=\begin{bmatrix}\tau_{\mathrm{HH}} & \tau_{\mathrm{HL}}\\ \tau_{\mathrm{LH}} & \tau_{\mathrm{LL}}\end{bmatrix} \quad \text{and} \quad \rho=\begin{bmatrix}\Gamma_{\mathrm{HH}} & \Gamma_{\mathrm{HL}}\\ \Gamma_{\mathrm{LH}} & \Gamma_{\mathrm{LL}}\end{bmatrix}. \tag{17}$$

The matrices $\tau'$ and $\rho'$ can be defined similarly by priming all the elements in Eq. (17). In the matrices above, the first index characterizes the hole character upon reflection or transmission, and the second index is a reminder of which hole is incident on the interface. The overall scattering matrix across the emitter-base junction is then obtained using the cascading rules for scattering matrices described in Ref. 21. As described above, the valence band must first be approximated by segmenting the potential-energy profile into a number of small intervals in which the potential is approximated as a constant. Intervals should be sufficiently small to represent the potential profile accurately. At the interface between steps, the scattering matrix must be determined as outlined above. For the regions where the valence band is approximated by a constant, the scattering matrices have only nonzero elements on the diagonal which are the corresponding phase shifts for the heavy and light holes as they transit across the regions.

In order to calculate the transmission and reflection coefficients for heavy and light holes incident from the left contact (see Fig. 1), the probability current density must be calculated along the growth direction (selected to be the $z$ axis). This expression has been derived previously,[15,24]

$$\begin{aligned} j_{z,\alpha}=\mathrm{Re}\,\frac{2}{\hbar}\{&[(|F_{1,\alpha}|^2+|F_{2,\alpha}|^2)\Gamma_1\\ &-(|F_{1,\alpha}|^2-|F_{2,\alpha}|^2)2\Gamma_2]k_{z,\alpha}\\ &+2i\sqrt{3}k_x\Gamma_3F_{1,\alpha}F_{2,\alpha}^{\dagger}\}, \end{aligned} \tag{18}$$

where $\alpha=H$ or $L$ for the incident heavy and light holes, respectively. Using Eq. (18), the transmission coefficients for a heavy hole incident from the left are calculated as follows:[24]

$$T_{\mathrm{HH}}=\frac{|\tau_{\mathrm{HH}}|^2 j_{z,H}^{\mathrm{trans}}}{j_{z,H}^{\mathrm{inc}}}, \quad T_{\mathrm{LH}}=\frac{|\tau_{\mathrm{LH}}|^2 j_{z,L}^{\mathrm{trans}}}{j_{z,H}^{\mathrm{inc}}}, \tag{19}$$

and the reflection coefficients are

$$R_{\mathrm{HH}}=-\frac{|\Gamma_{\mathrm{HH}}|^2 j_{-z,H}^{\mathrm{inc}}}{j_{z,h}^{\mathrm{inc}}}, \quad R_{\mathrm{LH}}=-\frac{|\Gamma_{\mathrm{LH}}|^2 j_{-z,L}^{\mathrm{inc}}}{j_{z,H}^{\mathrm{inc}}}. \tag{20}$$

where $\alpha=L$ and $H$ for the light and heavy holes, respectively. In Eqs. (19) and (20), the labels inc and trans mean that the probability current density must be evaluated in the incident and transmitted regions, respectively. Furthermore, the relationship $j_{-z,\alpha}=-j_{z,\alpha}$ holds between the probability current densities corresponding to left ($j_{-z,\alpha}$) and right ($j_{z,\alpha}$) propagating states. Current conservation further requires that $T_{\mathrm{HH}}+T_{\mathrm{LH}}+R_{\mathrm{HH}}+R_{\mathrm{LH}}=1$, which is helpful to check the accuracy of the numerical simulations.

Since we will be looking at the coherent transport of holes across the emitter-base junction of a $Pnp$ HBT under forward bias, we will only consider the case of heavy and light holes incident from the left contact hereafter. Finally, the formalism described above can be reworked easily while starting with the lower Hamiltonian in Eq. (4). In this case, the analysis outlined above must be repeated with the explicit forms of the eigenvectors of the lower Hamiltonian given in Table I of Ref. 27 and the appropriate boundary conditions.[26] For asymmetric structures, the transmission and reflection coefficients for heavy and light holes are known to be different while starting with either the upper or lower Hamiltonian in Eq. (4). This has been shown numerically by several authors,[17,18,20,24] while using a transfer-matrix approach to describe hole tunneling through resonant tunneling structures under bias. The transmission and reflection coefficients for holes through the highly asymmetric valence-band energy profile across the emitter-base junction of a typical HBT are therefore expected to be different while starting with the upper and lower Hamiltonian in Eq. (4). This will be illustrated in the numerical examples below for two typical $Pnp$ abrupt HBTs using $In_{0.52}Al_{0.48}As/In_{0.53}Ga_{0.47}As$ and $Al_{0.3}Ga_{0.7}As/GaAs$ heterostructures.

## III. RESULTS

For simplicity, we assume in all the numerical examples below that $k_y=0$. First, the valence-band energy profile for a given structure is computed as a function of the forward emitter-base bias using the program FISH1D.[28] We approximate a given valence-band energy profile as a series of small steps 10 Å wide. The valence-band energy profile in the emitter is used as the zero of energy and the valence-band energy is assumed to be constant throughout the heavily doped base. This amounts to neglecting the band bending in the base at the proximity of the emitter-base junction. This is a good approximation at large forward emitter-base bias as illustrated in Fig. 1. All calculations are performed assuming room-temperature operation for all devices.

*Example 1:* First, we study hole tunneling through the emitter-base junction of a $Pnp$ HBT similar to the one investigated by Hutchby.[29] The emitter consists of a 700-Å-long $P$-type $Al_{0.3}Ga_{0.7}As$ region doped at $2\times10^{17}$ cm$^{-3}$ on top of a 300-Å $Al_xGa_{1-x}As$ graded region with the same doping level. The graded region consists of two regions of $Al_xGa_{1-x}As$ with $x=0.2$ and 0.1 going from emitter to base, each region being 150 Å wide. The base region consists of a 600-Å heavily doped ($5\times10^{18}$ cm$^{-3}$) $N$-type region. For comparison, hole tunneling was also considered for an abrupt structure in which the emitter consists of 1000 Å of $P$-type $Al_{0.3}Ga_{0.7}As$ doped at $2\times10^{17}$ cm$^{-3}$, the rest of the structure being unchanged. The following Luttinger parameters were used: $\gamma_1=6.85$, $\gamma_2=2.1$, and $\gamma_3=2.9$ for GaAs, and $\gamma_1=3.45$, $\gamma_2=0.68$, and $\gamma_3=1.29$ for AlAs.[15] The corresponding values for $Al_xGa_{1-x}As$ were obtained by linear interpolation. For both structures, the valence-band energy profiles were calculated for $V_{\mathrm{EB}}$ ranging from 0 to 1.5 V, and the results are displayed in Fig. 1.

First, in Fig. 2 we plot the real ($\mathrm{Re}k_z^{(H)}$) and imaginary ($\mathrm{Im}k_z^{(H)}$) parts of the heavy-hole wave number $k_z^{(H)}$ in the $Al_{0.3}Ga_{0.7}As$ region as a function of energy for transverse wave vector $k_x$ equal to 0.04 ($2\pi/a$), where $a=5.65$ Å is the lattice constant of GaAs. Figure 2 also shows the corresponding real and imaginary parts of the light-hole wave number $k_z^{(L)}$ in GaAs. In Fig. 2, the zero of energy is the top of the valence band in the emitter region and the bias across the emitter-base junction is assumed to be 1.5 V. The critical energies ($E_h^-$, $E_h^+$, $E_1$) at which there is a sudden break in

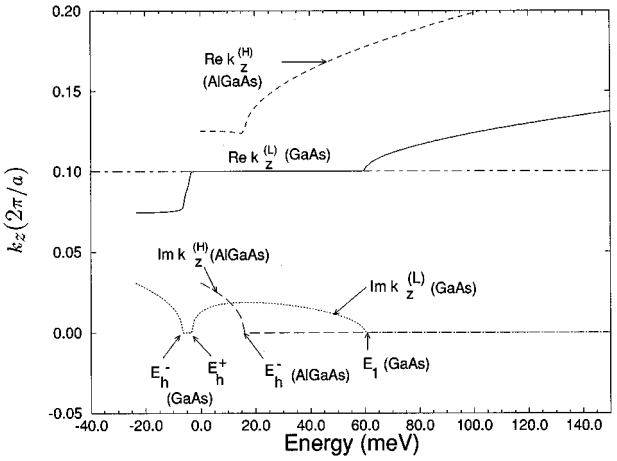


FIG. 2. Real and imaginary parts of the heavy-hole wave number $k_z^{(H)}$ in the $Al_{0.3}Ga_{0.7}As$ region as a function of energy for a value of $k_x=0.04\ (2\pi/a)$. Also shown are the real and imaginary parts of the light-hole wave vector in the GaAs region. A bias of 1.5 V was applied across the emitter-base junction of the structure considered. The zero of energy is the top of the valence band in the emitter region. The real and imaginary parts of both heavy and light holes are expressed in units of $2\pi/a$, where $a=5.65$ Å is the lattice constant of GaAs. For clarity, the real parts have been shifted vertically by an amount equal to 0.1 $(2\pi/a)$.

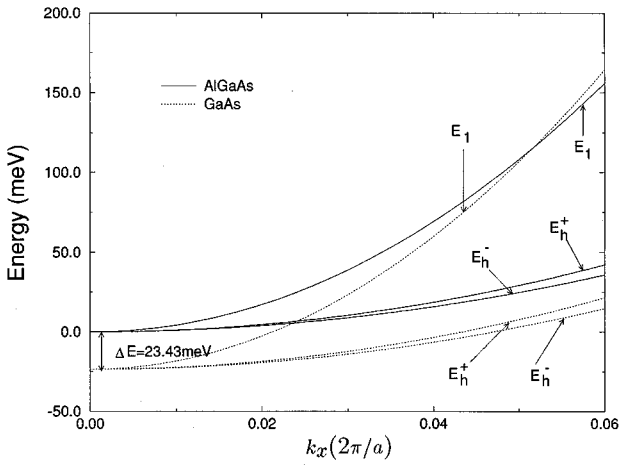


FIG. 3. Dependence of $k_x$ of the energies $(E_h^-, E_h^+, E_1)$. $\Delta E$ is the energy difference between the top of the valence band in the bulk of the emitter, and that in the base region for a bias $V_{EB}$ of 1.5 V across the $Al_{0.3}Ga_{0.7}As$ emitter-base junction considered.

the energy dependence of the real and imaginary wave-vector components of the heavy and light holes were calculated explicitly in Ref. 24. These expressions are repeated here for the sake of completeness:

$$E_1=(\gamma_1+2\gamma_2)\frac{\hbar^2k_x^2}{2m_0}, \tag{21}$$

$$E_h^+=(\gamma_1-2\gamma_2)\frac{\hbar^2k_x^2}{2m_0}, \tag{22}$$

and

$$E_h^-=\Gamma^+\frac{\hbar^2k_x^2}{2m_0}, \tag{23}$$

where

$$\Gamma^+=\frac{3}{2}\frac{\gamma_1(\gamma_3^2-\gamma_2^2)}{\gamma_2^2}\times\left\{-1+\left[1+\frac{4}{3}\frac{\gamma_2^2}{\gamma_1^2(\gamma_3^2-\gamma_2^2)}(\gamma_1^2-\gamma_2^2-3\gamma_3^2)\right]^{1/2}\right\}. \tag{24}$$

The $k_x$ dependence of the energies $(E_h^-, E_h^+, E_1)$ in the $Al_xGa_{1-x}As$ and GaAs regions for the HBT structure described above are plotted in Fig. 3. The energies $E_h^-, E_1$ are the energy thresholds for the existence of propagating heavy and light holes, respectively, as a function of $k_x$. The interval $(E_h^-, E_h^+)$ corresponds to a small range of energy for which $\mathrm{Re}k_z^{(L)}$ is negative while $\mathrm{Im}k_z^{(L)}$ is zero.[24] As discussed by Chao and Chuang,[17] within the energy range $(E_h^-, E_h^+)$, both roots of Eq. (6) for $k_z$ lie on the heavy-hole energy surface and there are no light-hole waves at all. In that case, labeling them $k_z^{(H)}$ and $k_z^{(L)}$ is just a matter of convenience.[17,24] From Fig. 2, we expect the probability of conversion from heavy to light hole while crossing an $Al_xGa_{1-x}As/GaAs$ interface to be small since, for a given energy above the threshold $E_1$ for light-hole propagation in GaAs, $\mathrm{Re}k_z^{(L)}$ in the GaAs region is much smaller in magnitude than $\mathrm{Re}k_z^{(H)}$ in the $Al_xGa_{1-x}As$ region.

The lack of efficiency for heavy- to light-hole conversion is illustrated in Figs. 4 and 5, where we plot the various reflection and transmission coefficients for a heavy hole incident from the emitter into the base in the abrupt HBT structure described above. The results in Figs. 4 and 5 are calculated using upper and lower Hamiltonians, respectively. In

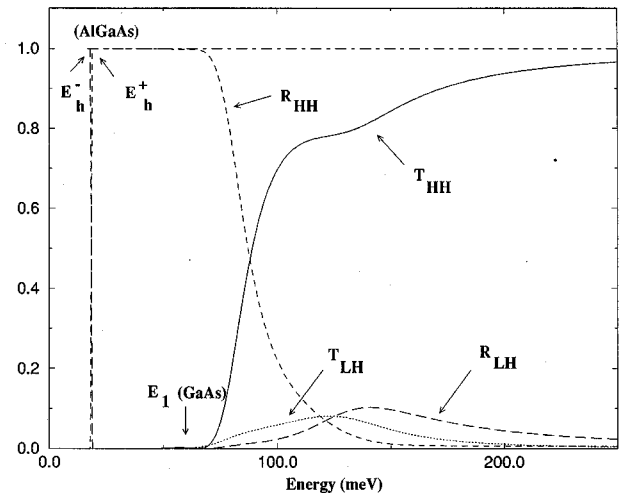


FIG. 4. Plot of the reflection $(R_{HH}, R_{LH})$ and transmission $(T_{HH}, T_{LH})$ coefficients for a heavy hole incident from emitter into base for $V_{EB}=1.5V$ and $k_x=0.04(2\pi/a)$. The results are for the upper Hamiltonian. The zero of energy is the maximum of the valence band in the emitter region. The location of the energy $E_1$ in the GaAs base above which free propagating holes exist in the base region is indicated. This threshold energy $E_1$(GaAs) increases for larger values of $k_x$, as indicated in Fig. 3.

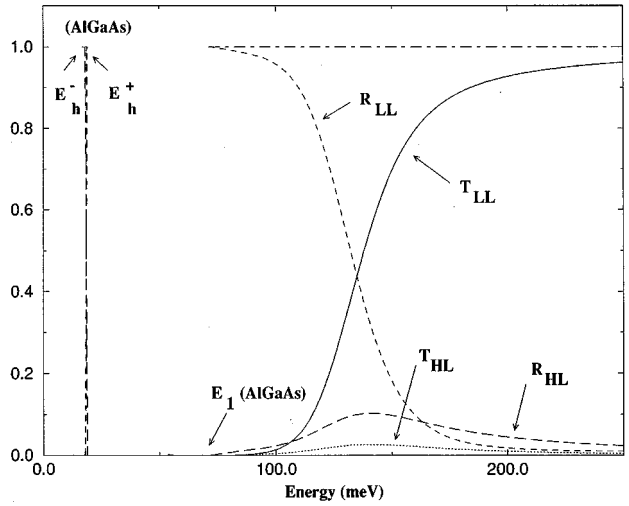


FIG. 5. Same as Fig. 4 for a light hole incident from the emitter. $E_1(\mathrm{Al}_x\mathrm{Ga}_{1-x}\mathrm{As})$ is the threshold energy for free propagating light holes in the emitter. There is no propagating light hole in the energy range $[E_h^+(\mathrm{Al}_x\mathrm{Ga}_{1-x}\mathrm{As})-E_1(\mathrm{Al}_x\mathrm{Ga}_{1-x}\mathrm{As})]$.

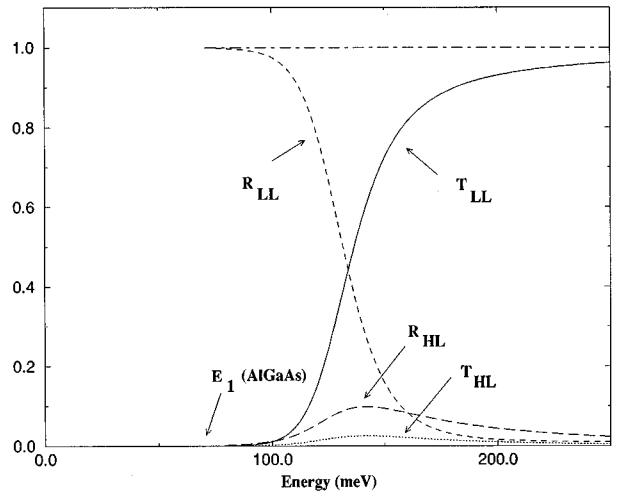


FIG. 7. Same as Fig. 5 for the lower Hamiltonian. The results are plotted for a total energy $E$ above $E_1(\mathrm{Al}_x\mathrm{Ga}_{1-x}\mathrm{As})$, the threshold energy for free propagating light holes in the emitter. The results are nearly identical to those obtained in Fig. 5 with the upper Hamiltonian.

both figures, $V_{\mathrm{EB}}$ was set equal to 1.5 V, and $k_x$ was chosen equal to 0.04 $(2\pi/a)$. The probability for conversion from heavy- to light-hole $T_{\mathrm{LH}}$ is nonzero only past the threshold energy $E_1(\mathrm{GaAs})$. Above that energy, $T_{\mathrm{LH}}$ reaches a maximum of 0.1 and 0.3 when the upper (Fig. 4) or lower (Fig. 5) Hamiltonians is used, respectively. In the energy range $(E_h^-, E_h^+)$, we found that $T_{\mathrm{LH}}$ and $T_{\mathrm{HH}}$ are negligible, and that $R_{\mathrm{LH}}+R_{\mathrm{HH}}=1$. Heavy holes incident within that range are therefore totally reflected while keeping their heavy-hole character. Indeed, as discussed above, both roots in Eq. (6) for $k_z$ lie on the heavy-hole energy surface within the energy range $(E_h^-, E_h^+)$.

Figures 6 and 7 show the reflection and transmission coefficients for an incident light hole calculated using the upper and lower Hamiltonians, respectively. The transmission probability $T_{\mathrm{LL}}$ is non-zero above the threshold energy $E_1(\mathrm{Al}_x\mathrm{Ga}_{1-x}\mathrm{As})$ for light-hole propagation in the emitter. As seen in Figs. 6 and 7, the probability of conversion from light to heavy holes is quite small while crossing the emitter-base interface from the emitter side. A comparison of Figs. 6 and 7 show that the energy dependence of the transmission and reflection coefficients for the light hole is nearly the same when calculated with the upper and lower Hamiltonians. We also found that $T_{\mathrm{HL}}$ and $T_{\mathrm{LL}}$ are negligible and $R_{\mathrm{HL}}+R_{\mathrm{LL}}=1$ within the energy range $(E_h^-, E_h^+)$, a result in agreement with the one observed in Fig. 4 for heavy-hole.

To illustrate the difference between abrupt and graded heterojunctions, in Fig. 8 we plot the energy dependence of the transmission coefficients $(T_{\mathrm{HH}}, T_{\mathrm{LH}}, T_{\mathrm{HL}}, T_{\mathrm{LL}})$ in the graded structure shown in Fig. 1, for $k_x$ equal to 0.04 $(2\pi/a)$. The transmission coefficients for heavy and light holes are calculated for the upper Hamiltonian only. A com-

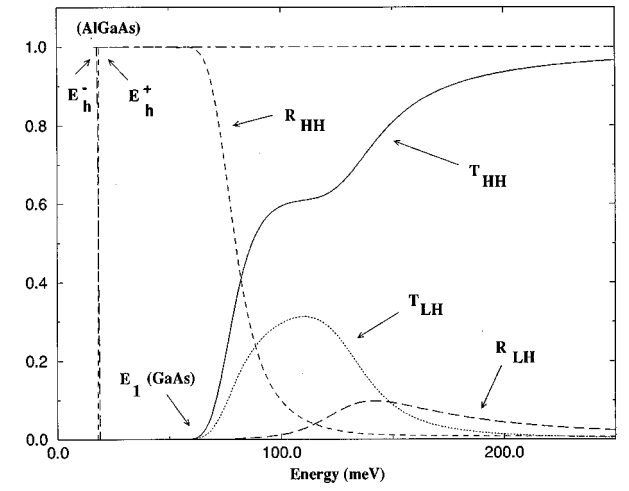


FIG. 6. Same as Fig. 4 for the lower Hamiltonian. The maximum of $T_{\mathrm{LH}}$ is around 0.3, compared to 0.1 in Fig. 4.

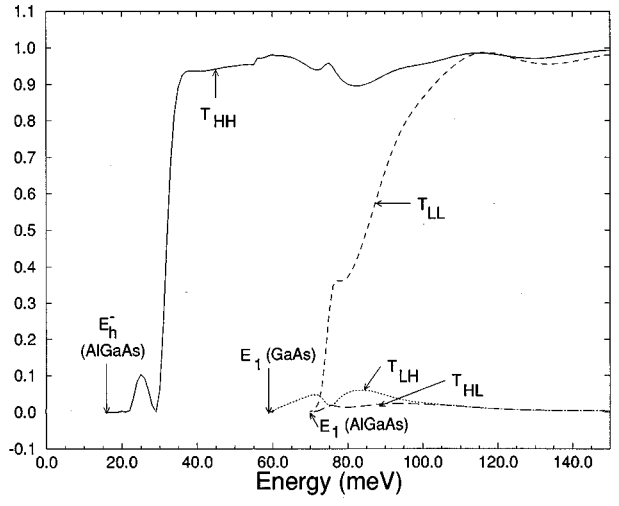


FIG. 8. Plot of the transmission coefficients $(T_{\mathrm{HH}}, T_{\mathrm{LH}}, T_{\mathrm{LL}}, T_{\mathrm{HL}})$ as a function of energy for a heavy hole incident from the emitter in the graded junction of Fig. 1. The results are for the upper Hamiltonian. The wave vector $k_x$ is equal to $0.04(2\pi/a)$. The emitter-base voltage is set to 1.5 V. The threshold energies $E_1(\mathrm{GaAs})$, $E_h^-(\mathrm{Al}_x\mathrm{Ga}_{1-x}\mathrm{As})$, and $E_1(\mathrm{Al}_x\mathrm{Ga}_{1-x}\mathrm{As})$ are shown in Fig. 3.

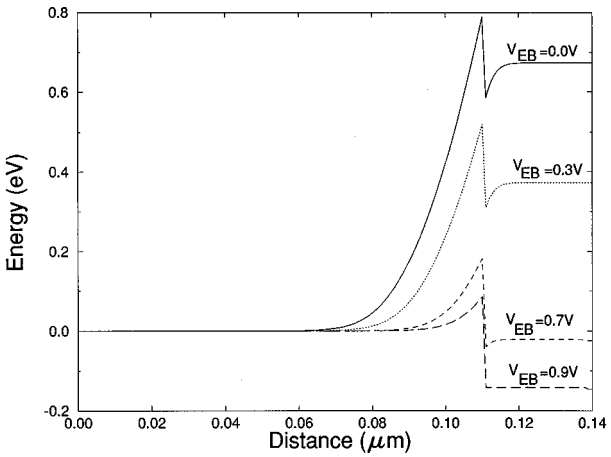


FIG. 9. Valence-band energy profile across the emitter-base junction of an InP-based abrupt $Pnp$ HBT. The emitter consists of a 1100 Å $P$-type $In_{0.52}Al_{0.48}As$ region doped at $8\times10^{17}$ cm$^{-3}$ on top of a 300-Å-wide base doped $N$ type at $7\times10^{18}$ cm$^{-3}$. The valence-band energy profile across the emitter-base junction was computed over a set of forward biases ranging from 0.0 to 0.9 V. Hole energies are measured positive, as indicated on the figure while taking the valence-band energy profile in the bulk of the emitter region as the zero of energy.

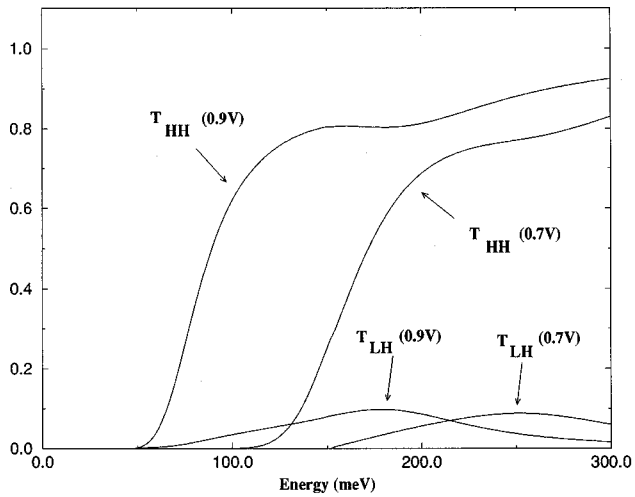


FIG. 10. Bias dependence of the transmission coefficients $T_{HH}$ and $T_{LH}$ for a heavy hole incident from the emitter across the abrupt $In_{0.52}Al_{0.48}As/In_{0.53}Ga_{0.47}As$ emitter-base junction described in example 2. The wave vector $k_x$ is equal to $0.04(2\pi/a)$. The results are for the upper Hamiltonian. The zero of energy is the maximum of the valence band in the emitter region. The results are for the upper Hamiltonian.

parison of Figs. 8 and 4 indicates that heavy- to light-hole conversion is as inefficient in a graded junction as in an abrupt junction. Though not shown here, the same conclusion was reached starting with the lower Hamiltonian. In a graded junction, the tunneling coefficient for heavy holes approaches unity much faster than in an abrupt junction and at lower energy, a feature similar to that observed for electrons crossing the emitter-base junction of graded versus abrupt $Npn$ HBT's at the same emitter-base bias. Since the heavy- to light-hole conversion is quite inefficient for holes crossing an emitter-base junction, abrupt junctions are more suited for $Pnp$ HBT's, since hole injection occurs at a higher energy in the base for the more predominant heavy-hole population incident from the emitter. This higher-energy distribution helps reducing the heavy-hole base transit time.

*Example 2:* We have repeated the simulations described in the previous example for an InP-based $Pnp$ transistor similar to the one recently fabricated in Ref. 8. The emitter consists of a 1100 Å $P$-type $In_{1-x}Al_xAs$ region doped at $8\times10^{17}$ cm$^{-3}$ on top of a 300-Å-wide base doped $N$ type at $7\times10^{18}$ cm$^{-3}$. The valence-band energy profile across the emitter-base junction was computed over a set of forward biases ranging from 0.0 to 0.9 V, and the results are displayed in Fig. 9. The following Luttinger parameters were used: $\gamma_1=6.85$, $\gamma_2=2.1$, and $\gamma_3=2.9$ for GaAs; $\gamma_1=20.4$, $\gamma_2=8.3$, and $\gamma_3=9.1$ for InAs;[27] and $\gamma_1=3.45$, $\gamma_2=0.68$, and $\gamma_3=1.29$ for AlAs. The corresponding values for $In_{0.52}Al_{0.48}As$ and $In_{0.53}Ga_{0.47}As$ were obtained by linear interpolation.

Figure 10 shows a plot of the tunneling coefficients $(T_{HH},T_{LH},T_{HL},T_{LL})$ versus energy for a fixed $k_x$ equal to 0.04 $(2\pi/a)$ for two different values of the emitter-base biases (0.7 and 0.9 V). The tunneling coefficients were calculated using the upper Hamiltonian. Figure 11 shows the results obtained with the lower Hamiltonian. For both biases, the zero of energy in Figs. 10 and 11 is the maximum of the valence band in the emitter region. As in the first example, the probability for hole conversion $(T_{LH})$ from heavy to light holes above the threshold energy $E_1$ in the $In_{0.53}Ga_{0.47}As$ region is larger (maximum equal to 37%) when calculated with the lower Hamiltonian. Above the threshold energy for heavy-hole propagation, the maximum of the transmission coefficients $T_{LH}$ and $T_{HL}$ is slightly increased at a larger forward emitter-base bias as a result of the reduction of the energy spike at the emitter-base junction as illustrated in Fig. 9.

*Effects of anisotropy:* Since the hole conversion seems to be of little significance for hole tunneling across either abrupt or graded emitter-base junctions, one last issue to be addressed is the importance of the anisotropy of both heavy and light holes on their tunneling probabilities. If there were no mixing nor anisotropy, the heavy and light holes could be

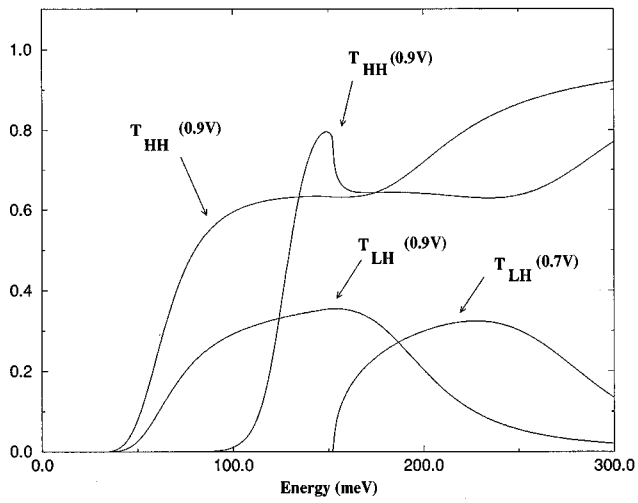


FIG. 11. Same as Fig. 10, for the lower Hamiltonian.

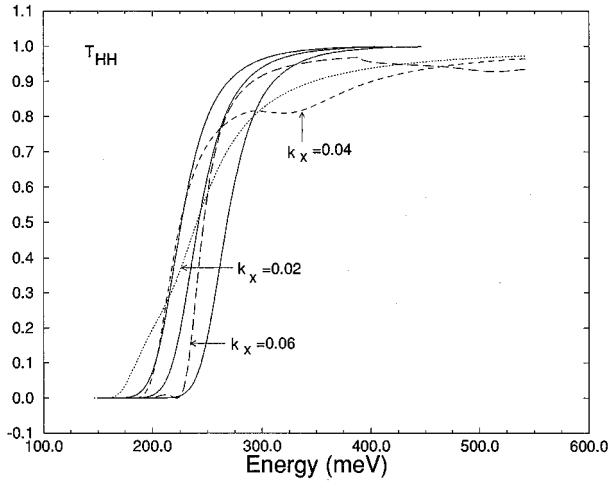


FIG. 12. Energy dependence of the transmission coefficient ($T_{HH}$) for heavy holes from emitter to base across the abrupt emitter junction of the $In_{0.52}Al_{0.48}As/In_{0.53}Ga_{0.47}As$ structure in example 2. The bias across the emitter-base junction is equal to 0.9 V. $T_{HH}$ is plotted as dashed lines for several values of $k_x$. The full lines are the heavy-hole transmission coefficients calculated in the parabolic band approximation. From left to right, the full lines correspond to $k_x=0.02$, 0.04, and 0.06 in units of $2\pi/a$. The results are shown for the upper Hamiltonian.

treated as independent particles with effective masses given by

$$m_{HH}=m_0/(\gamma_1-2\gamma_2), \tag{25}$$

$$m_{LH}=m_0/(\gamma_1+2\gamma_2), \tag{26}$$

respectively. This is referred as the parabolic band model hereafter.

For the $In_{1-x}Al_xAs/In_xGa_{1-x}As$ HBT considered above with $V_{EB}=0.9$ V, we compare in Figures 12 and 13 the tunneling coefficients for heavy ($T_{HH}$) and light holes ($T_{LL}$), respectively, calculated using the full $E-k$ relationship [Eq. (5)] and in the parabolic approximation for different values of $k_x$ (while assuming $k_y=0$). In Figs. 12 and 13, the zero of energy is the maximum of the valence band in the base region. A comparison of Figs. 12 and 13 shows that both $T_{HH}$ and $T_{LL}$ are sensitive to the value of $k_x$. This is due to the difference between the heavy- and light-hole effective masses in $In_{0.52}Al_{0.48}As$ ($m_{HH}=0.336m_0$, $m_{LH}=0.046m_0$) and $In_{0.53}Ga_{0.47}As$ ($m_{HH}=0.307m_0$, $m_{LH}=0.04m_0$). The fractional change across the interface for $m_{LH}$ is more important than for $m_{HH}$, which explains the less sensitive dependence of $T_{HH}$ on $k_x$. The $k_x$ dependence of $T_{LL}$ is quite dramatic, since the $k_x$ dependence of the threshold energy $E_1$ for light-hole propagation is more pronounced than the $k_x$ dependence of $E_h^-$, the threshold energy for heavy-hole propagation. Figure 13 shows that the parabolic band model is a fairly good approximation to the $k_x$ dependence of $T_{LL}$ obtained in the more complete $\mathbf{k}\cdot\mathbf{p}$ energy-band model. Conversely, the variation of the transmission coefficient $T_{HH}$ with energy in the $\mathbf{k}\cdot\mathbf{p}$ model is not as smooth as in the parabolic band model, an effect linked to the strong anisotropy of the heavy-hole energy dispersion relation in the $\mathbf{k}\cdot\mathbf{p}$ approximation. The $k_x$ dependence of $T_{HH}$ and $T_{LL}$ will affect the total transmitted current across the emitter-base junction. This was illustrated in the past in the case of electron tunneling through a structure with a variable effective mass,[30–32] and similar results are expected for holes. The calculation of the heavy- and light-hole emitter currents versus emitter-base bias will be published elsewhere.

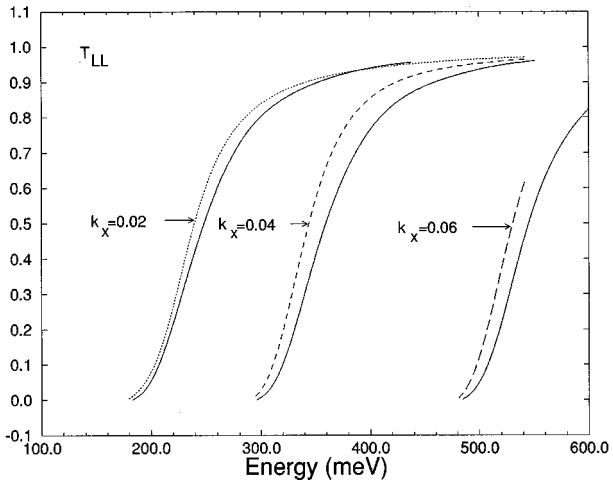


FIG. 13. Same as Fig. 12 for the transmission coefficient of light holes $T_{LL}$. From left to right, the full lines represent the light-hole transmission coefficients calculated in the parabolic band approximation for $k_x=0.02$, 0.04, and 0.06 in units of $2\pi/a$. The results are shown for the upper Hamiltonian. The zero of energy is the maximum of the valence band in the base region.

## IV. CONCLUSIONS

While neglecting the effects of the split-off band, we have used the $4\times4$ Luttinger-Kohn Hamiltonian and developed a scattering-matrix approach to study the effects of valence-band mixing and anisotropy on the tunneling of heavy and light holes across the emitter-base heterointerface of typical $Pnp$ heterojunction bipolar transistors. The tunneling and reflection coefficients of heavy and light holes were calculated for the upper and lower Hamiltonians obtained through a unitary transform of the $4\times4$ Luttinger-Kohn Hamiltonian.

For both abrupt and graded heterojunctions, the effects of mixing between the heavy and light holes appear only after the channel for light hole transmission opens up in the base region. Past that energy threshold, the probability for hole conversion is found to be more important for a heavy- to light-hole transition compared to the reverse for holes tunneling form emitter to base in both abrupt and graded $Pnp$ HBT's. For the $Al_{0.3}Ga_{0.7}As/GaAs$ ($In_{0.52}Al_{0.48}As/In_{0.53}Ga_{0.47}As$) abrupt HBT's analyzed here, the probability of heavy- to light-hole transition reaches a maximum around 10% (10%) and 30% (37%) in the simulations performed with the upper and lower Hamiltonians, respectively.

For practical $Pnp$ HBTs, the lack of efficient conversion from heavy to light holes for heavy holes incident from the emitter leads to an injection of carriers into the base mostly composed of heavy holes. The choice of an abrupt junction leads to injection of heavy holes at a higher energy in the base region, which helps in reducing the base transit time. The benefit of injecting the heavy holes across an abrupt

emitter-base junction for improving the high-frequency performance of $Pnp$ HBT's is in good agreement with the recent experimental results of Slater *et al.*[3] who reported a unity gain cutoff frequency of 33 GHz at a current density of $5.3\times10^4$ A/cm$^2$ in an $Al_{0.4}Ga_{0.6}As/GaAs$. In that structure, heavy holes are injected in a 325-Å-wide base with an energy close to a ramp energy of 196 meV (compared to 142 meV for an $Al_{0.3}Ga_{0.7}As/GaAs$ heterojunction) and the hole base transit time was estimated to be around 1.5 ps. Further improvement in the high-frequency performance of $Pnp$ HBT's would require eventually shortening the base region and/or using compositional grading in the base region to reduce the base transit time.

Finally, we have shown that the effects of anisotropy in the $E-k$ dispersion relation for holes have a profound effect on the parallel wave-vector dependence of the tunneling coefficients of heavy and light holes, the variation being quite drastic for light holes. The importance of anisotropy was illustrated by comparing heavy and light hole tunneling coefficients calculated in the $\mathbf{k}\cdot\mathbf{p}$ model to the results of a simple parabolic band model. The heavy- and light-hole currents injected across the emitter-base junction are therefore expected to be quite different from the results obtained using a simple parabolic band treatment. The light-hole component of the emitter current is expected to be much smaller than its heavy-hole counterpart since (1) the emitter is mostly populated with heavy holes, (2) the efficiency of the heavy- to light-hole conversion across the emitter-base junction is poor, and (3) the threshold energy for light-hole propagation in the base is much higher than for heavy holes. As a result, holes entering the base have a predominant heavy-hole character. This must have a profound effect on the base and collector transport of holes and so on $Pnp$ HBT's overall high-frequency performance. These issues will be addressed in a forthcoming publication.

## ACKNOWLEDGMENTS

This work was supported by the National Science Foundation (ECS-9525942). T.K. acknowledges support from the University Research Council at the University of Cincinnati. We also acknowledge the Ohio-Cray supercomputing center for the use of their facilities.

[1] M. E. Kim, B. Bayraktaroglu, and A. Gupta, in *HEMTs and HBTs: Device, Fabrication, and Circuits*, edited by F. Ali and A. Gupta (Artech, Boston, 1991), Chap. 5.
[2] P. M. Enquist, D. B. Slater, and J. W. Stuart, IEEE Electron Device Lett. **13**, 180 (1992).
[3] D. B. Slater, Jr., P. M. Enquist, A. S. Morris, and R. J. Trew, IEEE Electron Device Lett. **15**, 91 (1994).
[4] D. G. Hill, W. S. Lee, T. Ma, and J. S. Harris, IEEE Electron Device Lett. **11**, 425 (1990).
[5] W. Liu, D. Hill, D. Costa, and J. S. Harris, Electron. Lett. **26**, 200 (1990).
[6] J. F. Jensen, W. E. Stanchina, R. A. Metzger, D. B. Rensch, R. F. Lohr, R. W. Quen, M. W. Pierce, Y. K. Allen, and P. F. Lou, IEEE J. Solid-State Circuits **26**, 415 (1991).
[7] W. L. Chen, J. P. Sun, G. I. Haddad, M. E. Sherwin, G. O. Munns, J. R. East, and R. K. Mains, Appl. Phys. Lett. **61**, 189 (1992).
[8] W. E. Stanchina, R. A. Metzger, D. B. Rensch, L. M. Burns, J. F. Jensen, R. H. Walden, L. E. Larson, and P. T. Greiling (unpublished).
[9] L. M. Lunardi, S. Chandrasekhar, and R. A. Hamm, IEEE Electron Device Lett. **14**, 19 (1993).
[10] R. J. Ferro, R. G. Wilson, J. F. Jensen, D. B. Rensch, W. E. Stanchina, R. A. Metzger, M. W. Pierce, T. V. Kargodorian, and Y. K. Allen, Solid-State Electron. **34**, 1319 (1991).
[11] A. Das and M. S. Lundstrom, J. Appl. Phys. **66**, 2168 (1989).
[12] T. Kumar, M. Cahay, S. Shi, K. Roenker, and W. E. Stanchina, J. Appl. Phys. **77**, 5786 (1995).
[13] T. Kumar, M. Cahay, S. Shi, and K. Roenker, J. Appl. Phys. **78**, 6814 (1995).
[14] E. O. Kane, in *Physics of III-V Compounds*, edited by R. K. Willardson and A. C. Beer, Semiconductors and Semimetals, Vol. 1 (Academic, New York, 1966), p. 75.
[15] S. L. Chuang, Phys. Rev. B **40**, 10 379 (1989).
[16] R. Wessel and M. Altarelli, Phys. Rev. B **39**, 12 802 (1989).
[17] C. Y. Chao and S. L. Chuang, Phys. Rev. B **43**, 7027 (1991).
[18] J. B. Xia, Phys. Rev. B **38**, 8365 (1988).
[19] J. Lee, C. Jagannath, M. O. Vassell, and E. S. Koteles, Phys. Rev. B **37**, 4164 (1988).
[20] Y. X. Liu, D. Z.-Y. Ting, and T. C. McGill, Phys. Rev. B **54**, 5675 (1996).
[21] M. Cahay, M. McLennan, and S. Datta, Phys. Rev. B **37**, 10 125 (1988).
[22] P. F. Bagwell, Phys. Rev. B **41**, 10 354 (1990).
[23] D. Y. K. Ko and J. C. Inkson, Phys. Rev. B **38**, 9945 (1988).
[24] A. D. Sanchez and C. R. Proetto, J. Phys. Condens. Matter **7**, 2059 (1995).
[25] J. M. Luttinger and W. Kohn, Phys. Rev. **97**, 869 (1955).
[26] L. C. Andreani, A. Pasquarello, and F. Bassani, Phys. Rev. B **36**, 5887 (1987).
[27] S. L. Chuang, Phys. Rev. B **43**, 9649 (1991).
[28] The energy band diagram through the emitter-base junction is calculated using the program FISH1D released by Purdue University. Copies of the program can be obtained by contacting M. Lundstrom at lundstro@ecn.purdue.edu.
[29] J. A. Hutchby, IEEE Electron Device Lett. **EDL-7**, 108 (1986).
[30] A. A. Grindberg, Phys. Rev. B **33**, 7256 (1986).
[31] T. B. Boykin, J. Appl. Phys. **78**, 6818 (1995).
[32] T. B. Boykin, Phys. Rev. B **51**, 4289 (1995).